Transactions of the Nigerian Association of Mathematical Physics
Volume 10, **(***July and November, 2019***), pp119 – 126**

STRESS-STRAIN FAILURE ANALYSIS OF LIGHT-DUTY VEHICLE EXHAUST MATERIALS FOR OPTIMUM SERVICE PERFORMANCE

A.E. Ikpe and I.B. Owunna

Department of Mechanical Engineering, University of Benin, P.M.B. 1154

Abstract

This paper presents the analysis of different light-duty vehicle exhaust materials and their responses (in terms of stress, strain, displacement, fatigue etc.) to loading factors (temperature, vibration, corrosion etc.) of the exhaust system in service condition .The materials which included Cast Stainless steel, 1.4310 (X10CrNi18-8), Chrome Stainless Steel, Cast Alloy Steel, Stainless Steel Ferritic, Wrought Stainless Steel, Alloy Steel (SS), AISI 316L Stainless Steel and AISI 1020 Low Carbon Steel were analyzed with Solidworks software 2016 version using Finite Element Method (FEM).At maximum temperature of 900ºC Chrome Stainless Steel yielded the least Von-mises stress (152,564.258 N/mm^2) and equivalent strain (5.324e-009) followed by 1.4310 (X10CrNi18-8), while AISI 1020 Low Carbon Steel yielded the highest Von-mises stress (197,432.124 N/mm^2) and equivalent strain (7.236e-002). The study also revealed that Von-mises stress and equivalent strain increased as the exhaust temperature increased, thermal fatigue cycle increased as elastic strain increased and the fluctuating stress values increased as the natural frequency increased. Hence, Chrome Stainless Steel and 1.4310 (X10CrNi18-8) is the material of choice for light-duty exhaust systems due to their unyielding strength at extreme temperature, high resistance to corrosion and fatigue failure at high vibration frequency.

Keywords: Vehicle, Exhaust, Materials, Failure, Stress, Strain, Displacement

1. Introduction

Vehicle exhaust system is a vital component that is used in channeling the combusted exhaust gases from IC engine cylinder away from the engine. During operation, heat is dissipated as well as the emission of undesirable substances into the environment [1]. The choice of vehicle exhaust materials is driven by various factors such as cost, customer demands in terms of service performance and longevity, warranty requirements, emission policies etc. [2]. The application of plain carbon and low alloy steels on automotive exhaust systems had found its limitation in the mid-1990s, and have since been replaced primarily by stainless steel-based materials due to its excellent formability, high temperature strength and oxidation properties [3, 4]. The intricate technologies in automobile systems can influence its overall performance due to exhaust temperatures at the expense of exhaust material strength and durability as well as GHG emissions [5, 6]. Vehicle exhaust materials are exposed to temperature condition ranging from ambient to about 800ºC or even higher, and this can result in thermal fatigue failure which may translate into thermal stress prior to the material failure [7]. One of the stringent emission standards require that exhaust systems be designed in a manner that is leak-free, as this criterion if not met can constitute to GHG emissions and unwanted noise to the environment as well as unusual consumption of fuel [8, 9]. To meet the aforementioned criterion, ferrous alloys which are based on iron-carbon alloys such as carbon steel, alloy steels, stainless steel and cast iron have found their way into automobile exhaust design and manufacture. Also to enhance their service life, alloying elements are added which further advances their performance in service condition. This paper is focused on the analysis of different exhaust materials and their responses to the loading conditions during light-duty vehicle operation.

Correspondence Author: Ikpe A.E., Email: ikechukwu.owunna@uniben.edu, Tel: +2349034983495

2. Materials and Method

The analysis carried out in this paper was based on Finite Element Method (FEM) to examine the behavior of different exhaust materials during service condition. These materials were Cast Stainless steel, 1.4310 (X10CrNi18-8), Chrome Stainless Steel, Cast Alloy Steel, Stainless Steel Ferritic, Wrought Stainless Steel, Alloy Steel (SS), AISI 316L Stainless Steel and AISI 1020 Low Carbon Steel. As shown in Figure 1, The FEM modelling was done using Solidworks 2016 versions. The exhaust model was assumed as real live scenario of a light-duty vehicle whose service condition is subjected to thousands of vibrational cycle due to uneven road surface as well as extreme temperature condition. The mesh properties of the exhaust model are presented in Table 1.

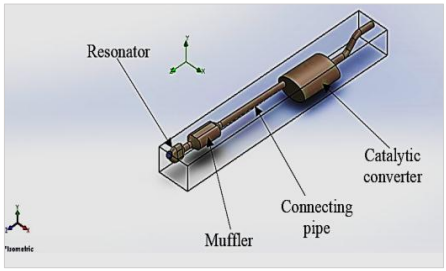

Figure 1: Model of the Exhaust System

Figure 2: Mesh Visualization of the Exhaust Model

Table 1: Mesh Properties of the Exhaust Model

Mesh type	Solid Mesh
Mesher Used	Curvature based mesh
Jacobian points	4 Points
Maximum element size	0.422394 in
Minimum element size	0.0844787 in
Total Nodes	66522
Total Elements	33823
Maximum Aspect Ratio	23.684
% of elements with Aspect Ratio < 3	58.9
% of elements with Aspect Ratio > 10	0.00591
Time to complete mesh (hh;mm;ss)	00:50:10
Total Nodes	66522

The mesh visualization of the light duty exhaust model is shown in Figure 2, with solid mesh being the mesh type represented. This is because for structural problems, each node in a solid element has three degree of freedom which represents the translations in three orthogonal directions (X, Y, Z) of the global Cartesian coordinate system. However, for thermally related problems like the exhaust systems, each node has one degree of freedom which is temperature. Curvature based mesh was also employed to control the mesh over high stress areas, and the maximum aspect ratio obtained was 23.684. Map meshing (mesh controller) as reported by Owunna and Ikpe[10] was applied on the exhaust model to improve the mesh performance by controlling aspect ratio of the nodal elements for consistent mesh.

2.1. Theoretical Background

The theoretical background and stress-strain equations governing the aforementioned exhaust materials under duty cycle is given as follows;

The in-service condition of the exhaust system is characterized by external loading conditions due to vibration, temperature, corrosion etc. and these conditions give rise to all form of deformations including stresses, strains as well as displacements on the exhaust material. The external load P is balanced by the internal resisting force $\sigma * dA$ within the material and this is given by the following relationship;

$$\left| \begin{array}{c} P = \sigma * dA \\ P = \sigma * dA = \sigma * A \\ \sigma = \frac{P}{A} \end{array} \right| \qquad (1)$$

Where, σ is the normal stress and A is the cross sectional area of the plane where the load acts upon. In tensor notation, the state of stress on the aforementioned plane is given by equation (2);

$$\sigma_{ij} = \begin{vmatrix} \sigma_{xx} & \sigma_{yx}\sigma_{zx} \\ \sigma_{xy}\sigma_{yy}\sigma_{zy} \\ \sigma_{xz}\sigma_{yz}\sigma_{zz} \end{vmatrix} \quad (2)$$

Where, i and j are iterated over x, y and z.

The average linear strain e is the ratio of the change in length, L, to the original length (L_o), given by equation (3);

$$e = \frac{\delta}{L_o} = \frac{\Delta L}{L_o} = \frac{L - L_a}{L_o} \quad (3)$$

In applications where the strain is too small, it can be referred to as infinitesimal normal strain which is the change in length, L, of a line given by equation (4);

$$d\varepsilon = \frac{dL}{L} \quad (4)$$

Integrating from the original length, L_o, to the final length, L, true strain is obtained as;

$$\varepsilon = \int \frac{dL}{L} = 1n\left(\frac{L}{L_o}\right) \quad (5)$$

Hooke's law elastic limit plays a role in this case, as the stress induced in the material is proportional to the strain at a given loading condition. This is given by equation (6)

$$\frac{\sigma}{e} = E = Constant \quad (6)$$

Where E is the modulus of elasticity also known as Young's Modulus.

In applications where the definition of strain (change in length) is referred to as the instantaneous length rather than to the original gauge length;

$$\varepsilon = \sum \frac{L_1 - L_O}{L_O} + \frac{L_2 - L_1}{L_1} + \frac{L_3 - L_2}{L_2} + \ldots\ldots \quad (7)$$

Or

$$\varepsilon = \int_{L_O}^{L} \frac{dL}{L} = 1n\frac{L}{L_o} \quad (8)$$

Considering thermal effects on the exhaust material as a result of the hot exhaust gases passing through it during operation, Hooks law becomes;

$$\sigma = E(\varepsilon - \alpha\Delta T) \quad (9)$$

Or the inverse,

$$\varepsilon = \frac{\sigma}{E} + \alpha\Delta T \quad (10)$$

Where, α is the coefficient of linear thermal expansion, ΔT is the change in temperature. For general non-uniaxial loads, the generalized Hook's law in equation (9) is further expressed as;

$$\bar{\bar{\tau}} = \frac{E}{1-v}\left(\bar{\bar{\varepsilon}} + \frac{v}{1-2v} tr(\bar{\bar{\varepsilon}})\bar{\bar{I}} - \frac{1+v}{1-2v}\alpha\Delta T\bar{\bar{I}}\right) \quad (11)$$

Or

$$\bar{\bar{\varepsilon}} = \frac{1-v}{E}\left(\bar{\bar{\tau}} + \frac{v}{1-2v} tr(\bar{\bar{\tau}})\bar{\bar{I}}\right) + \alpha\Delta T\bar{\bar{I}} \quad (12)$$

The relationship between true strain and conventional linear strain on the material is given by;

$$\begin{vmatrix} e = \frac{\Delta L}{L_o} = \frac{L - L_o}{L_o} = \frac{L}{L_o} - 1 \\ e + 1 = \frac{L}{L_o} \\ \varepsilon = 1n\frac{L}{L_o} = 1n\,(e+1) \end{vmatrix} \quad (13)$$

Consequently, the mean stress is given by the equation (14);

$$\sigma_m = \frac{\sigma_{axis}}{3} = \frac{\sigma_x + \sigma_y + \sigma_z}{3} = \frac{\sigma_1 + \sigma_2 + \sigma_3}{3} \quad (14)$$

The decomposition of the stress tensor is given by equation (15);

$$\sigma_{ij} = \sigma'_{ij} + \frac{1}{3}\delta_{ij}\sigma_{axis} \quad (15)$$

The elastic stress is linearly related to elastic strain via the Young's modulus given by equation (16);

$$\sigma_x = E\varepsilon_X \quad (16)$$

Thus, the stress-strain relationship in the x, y and z axis of the material is given by the following relationship;

$$\begin{vmatrix} \sigma_x\varepsilon_x = \frac{\sigma_x}{E} & \varepsilon_y = -\frac{v\sigma_x}{E} & \varepsilon_z = -\frac{v\sigma_x}{E} \\ \sigma_y\varepsilon_x = -\frac{v\sigma_x}{E} & \varepsilon_y = -\frac{\sigma_x}{E} & \varepsilon_z = -\frac{v\sigma_x}{E} \\ \sigma_z\varepsilon_x = -\frac{v\sigma_x}{E} & \varepsilon_y = -\frac{v\sigma_x}{E} & \varepsilon_z = -\frac{\sigma_x}{E} \end{vmatrix} \quad (17)$$

Where, σ_x, σ_y and σ_z are the stresses induced on the x, y and z axis of the material, ε_x, ε_y and ε_z denotes the strains on the x, y and z axis of the material, E is the Young's modulus and v denotes Poison's ratio which usually has a value close to 0.33 for most metals. By superposition of strain in the x, y and z axis, the following relationship is derived as;

$$\begin{vmatrix} \varepsilon_x = \frac{1}{E}\left[\sigma_x - v(\sigma_y + \sigma_z)\right] \\ \varepsilon_y = \frac{1}{E}\left[\sigma_y - v(\sigma_z + \sigma_x)\right] \\ \varepsilon_z = \frac{1}{E}\left[\sigma_z - v(\sigma_x + \sigma_y)\right] \end{vmatrix} \quad (18)$$

In extreme conditions where the vehicle is exposed to uneven road surfaces characterized by potholes, the exhaust system may be prone to cyclic loading which induces fluctuating stresses, tensile stress, strain etc. on the exhaust material that results in degradation of the material and possibly leads to fatigue. For a given material subjected to tensile stress along the x plane of the exhaust system for example, the elastic strain energy may be expressed mathematically as;

$$dU = \frac{1}{2}Pdu = \frac{1}{2}(\sigma_x A)(\varepsilon_x dx) = \frac{1}{2}(\sigma_x\, \varepsilon_x)(A\, dx) \quad (19)$$

The strain energy per unit volume also known as strain energy density U_o is given by equation (20);

$$U_o = \frac{1}{2}\sigma_x\, \varepsilon_x = \frac{1}{2}\frac{\sigma_x^2}{E} = \frac{1}{2}\varepsilon_x^2 E \quad (20)$$

In other words, the strain energy density per unit area of a given material subjected to pure shear is given by equation (21);

$$U_o = \frac{1}{2}\tau_{xy}\, \gamma_{xy} = \frac{1}{2}\frac{\tau_{xy}^2}{G} = \frac{1}{2}\tau_{xy}^2 G \quad (21)$$

According to Budynas and Nisbeth [11], a tensile stress field can contribute immensely to mode I crack propagation. Considering a mode I crack of length 2a in an infinite plate of a given exhaust material, the stress field in the domain of the crack tip can be derived from the following complex stress functions;

$$\sigma_x = \sigma\sqrt{\frac{a}{2r}}cos\frac{\theta}{2}\left(1 - sin\frac{\theta}{2}sin\frac{3\theta}{2}\right) \quad (22a)$$

$$\sigma_y = \sigma\sqrt{\frac{a}{2r}}cos\frac{\theta}{2}\left(1 + sin\frac{\theta}{2}sin\frac{3\theta}{2}\right) \quad (22b)$$

$$\tau_{xy} = \sigma\sqrt{\frac{a}{2r}}sin\frac{\theta}{2}cos\frac{\theta}{2}cos\frac{3\theta}{2} \quad (22c)$$

$$\sigma_z \begin{cases} 0 & (for\ plane\ stress) \\ v(\sigma_{x+}\sigma_{\ y})\ (for\ plane\ strain) \end{cases} \quad (22d)$$

The stress σ_y near the tip, with θ = 0 is given by equation (23). In expressions like this, it is a common practice to introduce factor K known as the stress intensity factor given by equation(24);

$$\sigma_y \Big| \theta = 0 = \sigma\sqrt{\frac{a}{2r}} \quad (23)$$

$$K = \sigma\sqrt{\pi a} \quad (24)$$

Since this analysis is based on mode I crack, equation (24) can be rewritten as equation (25). Equation (22a-c) can be rewritten as equation (26a-c).

$$K_I = \sigma\sqrt{\pi a} \quad (25)$$

$$\sigma_x = \frac{K_I}{\sqrt{2\pi r}}cos\frac{\theta}{2}\left(1 - sin\frac{\theta}{2}sin\frac{3\theta}{2}\right) \quad (26a)$$

$$\sigma_y = \frac{K_I}{\sqrt{2\pi r}}cos\frac{\theta}{2}\left(1 + sin\frac{\theta}{2}sin\frac{3\theta}{2}\right) \quad (26b)$$

$$\tau_{xy} = \frac{K_I}{\sqrt{2\pi r}}sin\frac{\theta}{2}cos\frac{\theta}{2}cos\frac{3\theta}{2} \quad (26c)$$

Von Mises (1913) proposed that yielding is likely to occur when the second invariant of stress deviator J2 exceeds some critical value. Therefore, $J_2 = K^2$.

$$J_2 = \frac{1}{6}[(\sigma_1 - \sigma_2)^2 + (\sigma_2 - \sigma_3)^2 + (\sigma_3 - \sigma_1)^2] \quad (27)$$

To evaluate the constant K and relate it to yielding of the material subjected to tensile loading in its service condition, then, at yielding in uniaxial tension, $\sigma_1 = \sigma_0$, $\sigma_2 = \sigma_3 = 0$.

$$\sigma_0^{\ 2} + \sigma_0^{\ 2} = 6K^2 \quad (28a)$$

$$\sigma_0 = \sqrt{3K} \quad (28b)$$

Substituting equation (28a)into equation (28b) gives the Von Mises yield criterion in equation (29);

$$\sigma_2 = \frac{1}{\sqrt{2}}[(\sigma_1 - \sigma_2)^2 + (\sigma_2 - \sigma_3)^2 + (\sigma_3 - \sigma_1)^2]^{1/2} \quad (29)$$

3. Results and Discussion

Figure 3 shows the flow trajectory of exhaust temperature which actually represent the heat transferred across the exhaust material. Severity of the heat on the exhaust material is a function of the exhaust temperature and can be fully understood from the color profile shown in Figure 3.

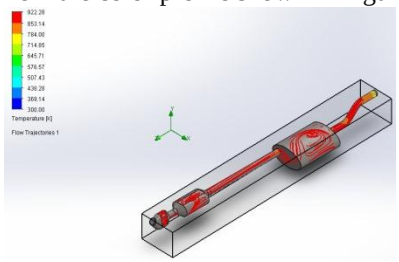

Figure 3: heat transfer across the exhaust material

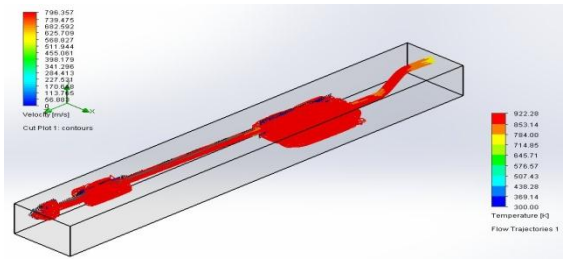

Figure 4: Flow Trajectory of Exhaust Temperature on the material

As shown in Figures 3, and other finite element models in this study, red color indicates the highest temperature distribution on the exhaust material, royal blue indicates the minimum temperature on the material, sky blue indicates the temperature at which the exhaust material begins to respond to the hot exhaust gases, aqua (SVG) blue indicates further responses of the welded metal from the temperature signified by the sky blue color etc. Each material has its own thermal properties which thermal expansion and melting temperature is one of such properties. In other words, as the exhaust temperature increase, so does the thermal expansion of the material due to increase in specific heat (Cp) in the exhaust gases which disorientate the atoms and electrons in the metal lattice [12]. As the exhaust material continues to absorb heat from the hot exhaust temperature, a point is reached where the material is thermally saturated and begins to fail. This type of failure is characterized by thermally induced stress and strain which is graphically represented in further analysis in this paper. Ideally in exhaust systems, it is rare or almost impossible to have peak exhaust temperature exceeding melting temperature of the exhaust materials. However, in situation where such event occurs, it implies that the exhaust material will undergo catastrophic failure in the form of melting which may not only cause damages to the vehicle but can result in the loss of lives depending on the severity. This is one of the major reasons why auto makers pay much attention to the selection of exhaust material. Figure 4 shows the flow trajectory of exhaust temperature in road condition at different velocities along the internal walls of the exhaust pipe.

Considering the red color distributed throughout the exhaust pipe in Figure 4, it can be seen that the exhaust material is completely at peak temperature. Ideally in real vehicle operation, peak temperature is obtained at road load condition not at idle mode, and it has some relationship with the engine speed (RPM), engine load as well as the volume of exhaust gas flowing through the exhaust pipe. Furthermore, a relationship can be established considering the numerical trend of exhaust temperature and velocity (see Figure 4) which signifies that the higher the exhaust temperature, the more the velocity of the exhaust gases.

Figure 5 represents a graph of Von-mises stress against exhaust temperature. It can be observed that that for each material plotted, the von-mises stress distribution increases as the exhaust temperature increases. The Von-mises stress in this case can be considered as thermal stress due to the role played by the hot exhaust gases. Thermal stress on vehicle exhaust system is as a result of cyclic material expansion and contraction when there are changes in the exhaust temperature condition under geometric constraints. Depending on the heat intensity, the exhaust material can experience great reduction in strength as well as thermal conductivity. According to Owunna and Ikpe[13], metal exposure to intense temperature can result in the loss of electron flow, thereby, reducing its thermal conductivity.

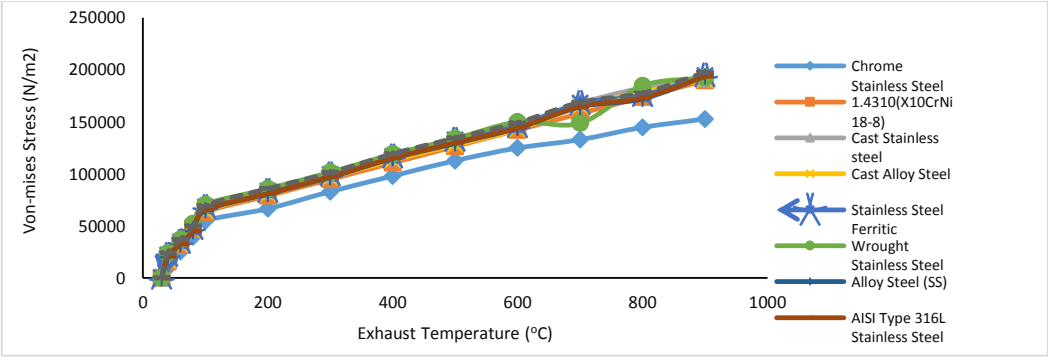

Figure 5: Plot of Von-mises Stress against Exhaust Temperature

Figure 6 represents a graph of equivalent strain against exhaust temperature. Like the case of Von-mises stress in Figure 5, It can be observed that for each exhaust material in the graph, equivalent strain increases as the exhaust temperature increases and vice versa. This is due to the thermal expansion coefficient which is the equivalent strain divided by the change in temperature. Hence, for exhaust materials with low coefficient of thermal expansion, their distortion rate in response to changes in exhaust temperature is also low. This causes an increase in strain along the bonded area within the atoms in the metal lattice as the exhaust temperature increases during service condition.

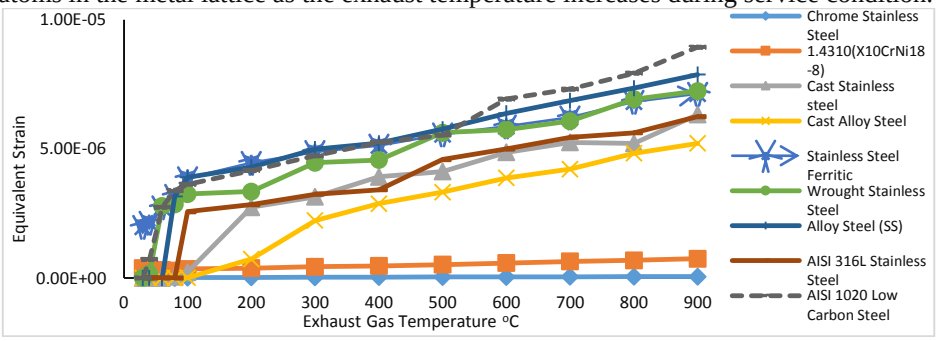

Figure 6: Plot of Equivalent Strain against Exhaust Temperature

One of the failure modes that a vehicle exhaust system is usually subjected to is thermal fatigue which occurs as a result of constant exposure of the exhaust material to the high temperature combusted gases expelled from the engine. Thermal fatigue is a type of failure that is characterised by microscopic cracks due to cyclic thermal stresses and strains resulting from temperature variation, spatial temperature gradients as well as extreme temperatures under constrained thermal deformation. However, Qianfan [14] reported that thermal failure is usually indicated by strain rather than stress. Figure 7 represents a graph of thermal fatigue cycle against elastic strain. In this case, a light duty vehicle exhaust temperature ranging from ambient to as high as 900^{o}C was considered.

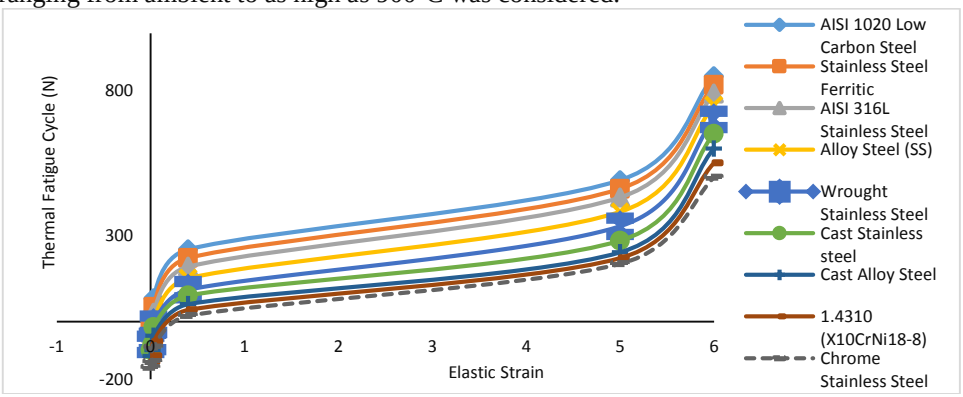

Figure 7: Plot of Thermal Fatigue Cycle against Elastic Strain

It can be observed from the graph in Figure 7 that the thermal fatigue cycle increased as the elastic strain also increased which are both disadvantageous to the service life of the exhaust material. The increase in both parameters is as a result of continuous increase in the exhaust temperature. The implication is that the mechanical properties of the exhaust material begins to deteriorate or fail when exposed above certain temperature limit, causing decrease in ultimate tensile strength of the material. This phenomenon can result in the occurrence of plastic deformation in the exhaust material.

In real life scenario, the exhaust system of a light-duty vehicle during operation is subjected to variable or alternating loads also referred to as fluctuating or fatigue loads which are attributed to the vibratory effect of the vehicle on the exhaust system. This is characterised by upward and downward movement as the vehicle goes through uneven road surface. The effect of such action can expose the exhaust material to fluctuating stress which triggers failure at stress level much lower than the ultimate strength of the material and in some cases lower than the yielding point of the material. The aforementioned failures occur as a result of extremely large cycles of stress, and are referred to as fatigue failure. This type of failure usually begins with pin hole crack which may occur at any point of discontinuity, existing subsurface crack or surface faults on the exhaust material.Figure 8 represents a graph of fluctuating stress against frequency. It can be observed that the trend of the graph is sinusoidal in nature. In this case, the fluctuating stress increases and decreasing as the natural frequency progresses.

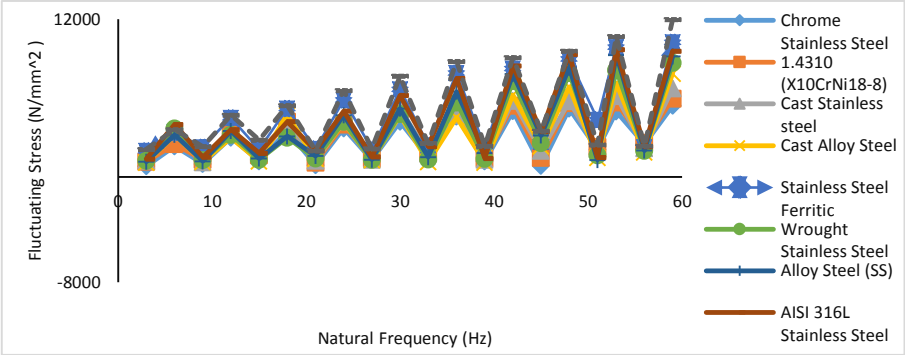

Figure 8: Plot of Fluctuating Stress against Natural Frequency

It should be noted that once a crack develops on the vehicle exhaust material, it propagates as stress cycle increases and eventually result in fracture of the exhaust material. This type of failure after crack initiation is characterised by progressive development of crack and unforeseen fracture without any sign. Failure caused by fatigue is influence by the magnitude of stress cycle as well as the endurance limit of the material. From the simulation carried out in this study, summary of maximum stress, maximum strain and maximum displacement for each exhaust materials are presented in Table 2.

Table 2: Design Study Showing Maximum Stress, Strain and Displacement for each Material

Material Name	**Units**	**Material 1**	**Material 2**	**Material 3**
Material	N/A	1.4310 (X10CrNi18-8)	Chrome Stainless Steel	Cast Stainless steel
Stress	N/mm^2 (MPa)	189,655.453	152,564.258	191,543.216
Strain		7.482e-007	5.324e-009	6.324e-006
Displacement	mm	5.362e-004	3.462e-008	4.193e-003
Material Name	**Units**	**Material 4**	**Material 5**	**Material 6**
Material	N/A	Cast Alloy Steel	Stainless Steel Ferritic	Wrought Stainless Steel
Stress	N/mm^2 (MPa)	190,345.254	194,326.347	192,432.124
Strain		5.212e-006	7.132e-004	7.236e-005
Displacement	mm	4.249e-003	4.351e-002	4.463e-003
Material Name	**Units**	**Material 7**	**Material 8**	**Material 9**
Material	N/A	Alloy Steel (SS)	AISI 316L Stainless Steel	AISI 1020 Low Carbon Steel
Stress	N/mm^2 (MPa)	193,436.362	193,652.436	197,432.124
Strain		7.873e-005	6.246e-005	7.236e-002
Displacement	mm	4.368e-002	5.726e-002	4.463e-001

Figure 9-11 represents the simulated result of exhaust models of two (2) different materials (Chrome Stainless Steel and 1.4310 (X10CrNi18-8)) with the list maximum stress, strain and displacement among the nine (9) exhaust materials analysed in this study.

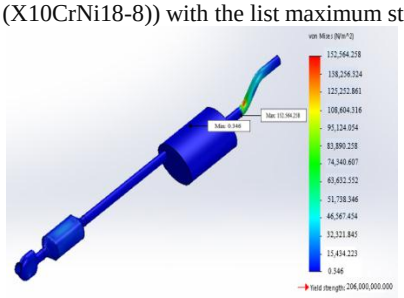

Figure 9a: Von-mises Stress on Chrome Stainless Steel

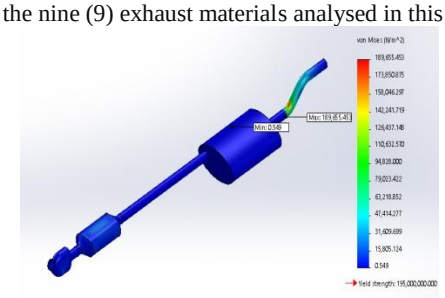

Figure 9b:Von-mises Stress on 1.4310 (X10CrNi18-8)

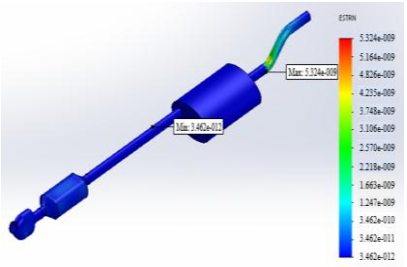

Figure 10a: Equivalent Strain on Chrome Stainless Steel

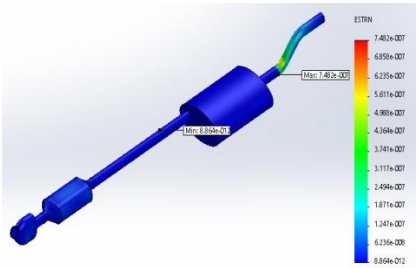

Figure 10b:Equivalent Strain on 1.4310 (X10CrNi18-8)

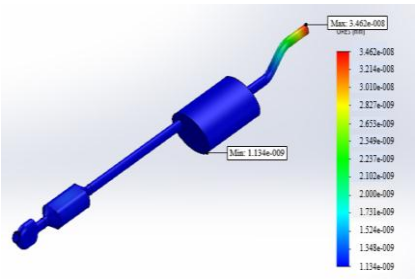

Figure 11a: Resultant Displacement on Chrome Stainless Steel

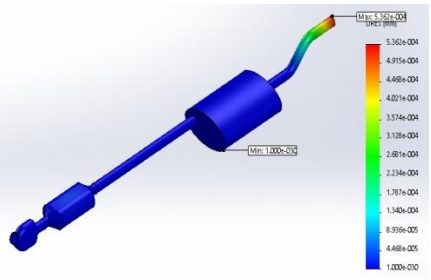

Figure 11b: Resultant Displacement on 1.4310 (X10CrNi18-8)

4. Conclusion

Nine (9) potential exhaust materials including Cast Stainless steel, 1.4310 (X10CrNi18-8), Chrome Stainless Steel, Cast Alloy Steel, Stainless Steel Ferritic, Wrought Stainless Steel, Alloy Steel (SS), AISI 316L Stainless Steel and AISI 1020 Low Carbon Steel were analyzed in this study using FEM approach. Each of the exhaust materials exhibited different behavior in response to the loading conditions particularly temperature and vibration at variable frequencies. The study clearly revealed that Chrome Stainless Steel and 1.4310 (X10CrNi18-8) among the nine (9) materials analyzed in this study were quite minimum in terms of thermal conditions, stress, strain and displacement criteria which is paramount in the longevity and service performance of light-duty exhaust materials. Hence, materials with high stress-strain cycles such as AISI 1020 low car steel in this study should be avoided in exhaust applications to prevent untimely failure that may result in loss of lives and properties.

References

[1] Saravanan, J., Valarmathi, T. N. Rajdeep, N. and Kumar, P. (2017) Experimental Analysis of Exhaust Manifold with Ceramic Coating for Reduction of Heat Dissipation. IOP Conference Series: Material Science and Engineering, 197, 012051.

[2] Rajadurai, S., Afnas, M., Ananth, S. and Surrendhar, S. (2014) Materials for Automotive Exhaust Systems. International Journal of Recent Development in Engineering and Technology, 2(3), 82-89.

[3] Inove, Y. and Kikuchi, M. (2003) Present and Future Trends of Stainless Steel for Automotive Exhaust Systems. Nippon Steel Technical Report, No. 88.

[4] Miyazaki, A., Hirasawa, J. and Furukimi, O. (2004) Ferritic Stainless Steel for Automotive Exhaust Systems-High Heat Resistance Ferritic Stainless Steel with High Formability for Automotive Exhaust Manifold: JFE-MHI. JFE Technical Report No. 4, May 2004, 53-57.

[5] Zimmermann, K. (2011) Light Weight Design in Exhaust Systems using Tailored Products. 9th International CTI Forum Exhaust Systems, January 26, 2011, Stuttgart, Germany.

[6] Borole, S. B. and Shah, G. V. (2016) Design Modification and Analysis of Engine Exhaust Manifold. International Research Journal of Engineering and Technology, 3(9), 210-220.

[7] Sarda, S. and Bindu, R. (2014) Exhaust Transfer Connection Material Selection Meeting Criteria Qualification Requirement in Automobile Application. International Journal of Mechanical and Production Engineering, 2(6), 87-91.

[8] Ganji, R. and Yenugula, V. N. (2017) Emission Reduction in Automobile Engine Exhaust Using Bio-Catalytic Converter: An Experimental Study. IOSR Journal of Mechanical and Civil Engineering, 14(16), 24-28.

[9] Williams, M. and Minjares, R. (2016) A Technical Summary of Euro 6/VI Vehicle Emission Standards. The International Councilon Clean Transportation (ICCT).

[10] Owunna, I. B. and Ikpe, A. E. (2019) Modelling and Prediction of Triboligical Ball Joint Failure Under Forced Vibration Scenario in Automobile Suspension System. Transactions of Nigerian Association of Mathematical Physics, 8, 145-152.

[11] Budynas, R. G. and Nisbett, J. K. (2008) Shigleys, Mechanical Engineering Design, Eighth Edition, McGraw-Hill, New York, ISBN: 978-007-126896-7.

[12] Owunna, I., Ikpe, A. E. and Achebo, J. I. (2018) Temperature and Time Dependent Analysis of TungstenInert Gas Welding of Low Carbon Steel Plate using Goldak Model Heat Source. Journal of Applied Science and Environmental Management, 22(11), 1719-1725.

[13] Owunna, I. B. and Ikpe, A. E. (2018) Effects of Parametric Variations on Bead Width of Gas Tungsten Arc Welding of AISI 1020 Low Carbon Steel Plate. International Journal of Engineering Technology and Sciences, 5(3), 1-13.

[14] Qianfan, X. (2016) Diesel Engine System Design. Woodhead Publishing, ISBN-13-978-0081016916.